X-ray magnetic circular dichroism studies of (001)-oriented NiFe/$Mn_{100-x}Pt_x$ exchange bilayers

T. Yamato, T. Kume, T. Kato,[a] and S. Tsunashima
Department of Electronics, Nagoya University, Furo-cho, Chikusa-ku, Nagoya 464-8603, Japan

T. Nakamura
SPring-8/JASRI, 1-1-1 Kouto, Mikazuki-cho, Sayo-gun, Hyogo 679-5198, Japan

Y. Fujiwara
Department of Physics Engineering, Mie University, 1515 Kamihama-cho, Tsu, Mie 514-8507, Japan

S. Iwata
CCRAST, Nagoya University, Furo-cho, Chikusa-ku, Nagoya 464-8603, Japan

(Received 27 February 2006; accepted 7 September 2006; published online 12 December 2006)

(001)-oriented $Ni_{80}Fe_{20}/Mn_{100-x}Pt_x$ and $Co_{90}Fe_{10}/Mn_{100-x}Pt_x$ epitaxial bilayers were prepared using the molecular beam epitaxy method. Their exchange anisotropies were measured using a torque magnetometer, while their interfacial Mn uncompensated moments were measured by means of x-ray magnetic circular dichroism. The bilayers exhibited both one- and fourfold components in their anisotropy torque curves, which are difficult to explain using a simple model assuming the coherent rotation of ferromagnetic (F) and antiferromagnetic (AF) spins. Uncompensated Mn moments were confirmed to exist in the $Mn_{100-x}Pt_x$ layer due to exchange coupling with the adjacent F layer, and the Mn moment of $CoFe/Mn_{100-x}Pt_x$ was found to be larger than that of $NiFe/Mn_{100-x}Pt_x$. In order to understand the experimental results, we extended the Mauri *et al.* [J. Appl. Phys. **62**, 3047 (1987)] domain wall model by assuming cubic anisotropy in the AF and four AF domains whose interfacial moments are oriented along the principal axis of (001)-oriented Mn–Pt. The model predicted the uncompensated AF moment resulting from the domain wall formed in the AF layer and well reproduced the coexistence of one- and fourfold anisotropies in the in-plane torque curves. The uncompensated moment and torque curve were found to be dependent on the ratio of F/AF interfacial exchange coupling and the AF domain wall energy. By changing the ratio, it was possible to reproduce exchange anisotropy for various systems, such as NiFe/MnPt, NiFe/MnIr, and CoFe/MnPt.
 [DOI: 10.1063/1.2388136]

I. INTRODUCTION

Exchange biasing at the ferromagnet (F)/antiferromagnet (AF) interface plays an important role in spin valve magnetic heads and magnetic random access memories (MRAMs). Despite its technological importance, the mechanism of exchange biasing remains unclear even though both extensive experimental and theoretical studies have been carried out.[1–9] Various theoretical models have been proposed to explain the experimental results of exchange coupling at the interface between F and AF layers. Meiklejohn and Bean first discussed exchange biasing by assuming a phenomenological interface exchange coupling at the F/AF interface and the coherent rotation of AF spins throughout the reversal of F magnetization.[3] According to their model, exchange biasing arises as a result of the competition of F/AF interface coupling and AF anisotropy energies, successfully explaining the onset of the exchange biasing below the AF Néel temperature and above the critical AF thickness. Most experimental studies have used or modified this model to understand their experimental results, such as temperature, thickness, and the directional dependences of exchange biasing.[10–12] Other theoretical models have been proposed to describe exchange coupling both qualitatively and quantitatively. Mauri *et al.* proposed the formation of an AF domain wall parallel to the interface by switching the adjacent F magnetization.[4] Malozemoff introduced random exchange coupling due to surface roughness.[5] Koon[6] and Shulthes and Butler[7] tried to interpret exchange biasing in terms of a 90° coupling between F and AF interfacial spins. However, the difficulty in probing the magnetic properties of AF leads to difficulty in discussing exchange coupling at the F/AF interface.

X-ray magnetic circular dichroism (XMCD) is a useful method to access the interface, since it reveals the element-specific magnetic moments of the F/AF bilayers. Recently, total electron yield (TEY) detection of the XMCD signal was reported to be useful in probing uncompensated AF spins at the F/AF interface.[13,14] Uncompensated spins are considered to be due to the AF domain wall formed near the F/AF interface[4,9] or an imbalance of AF spins at the interface.[15] This relationship between the observed uncompensated moment and exchange biasing is a subject of controversy.

We have studied the exchange anisotropies of epitaxially grown exchange bilayers as a means to investigate the relationship between the AF crystallographic orientation and the

[a]Electronic mail: takeshik@nuee.nagoya-u.ac.jp

exchange anisotropy. Recently, we have presented a study addressing (001)-oriented top-type $Mn_{100-x}Pt_x$/NiFe epitaxial bilayers, "top type" meaning that the NiFe was deposited prior to the MnPt layer.[16,17] The bilayers show an exchange bias field without heat treatment at Pt content x around 10 at. %, although well-known $Mn_{50}Pt_{50}$/F bilayers usually require heat treatment to obtain an antiferromagnetic ordered phase and the resulting large exchange bias field. Moreover, the (001)-oriented $Mn_{90}Pt_{10}$/NiFe exhibited both strong one- and fourfold anisotropies in its in-plane torque curve.[17] This fourfold anisotropy is considered to result from the cubic anisotropy of antiferromagnetic $Mn_{100-x}Pt_x$.

In the present study, we have measured Mn XMCD for "bottom-type" NiFe/$Mn_{100-x}Pt_x$ and CoFe/$Mn_{100-x}Pt_x$ bilayers using a surface-sensitive TEY method to detect uncompensated Mn spins. We observed the uncompensated Mn moment coupled with the adjacent ferromagnetic layer, this moment varying both with Pt content x in the AF and with the adjacent ferromagnetic material. We introduced an extended Mauri's model (domain wall model) which assumes cubic anisotropy in the AF and four AF domains whose interfacial moments are oriented along the principal axis of (001)-oriented Mn–Pt. This model predicts the variation of the observed uncompensated moments and explains the relationship between the exchange anisotropy at the F/AF interface and uncompensated Mn spins. Moreover, the model reproduced the observed in-plane torque curve both qualitatively and quantitatively.

II. EXPERIMENT

In this study, bottom-type $Ni_{80}Fe_{20}$ or $Co_{90}Fe_{10}$ (3 nm)/$Mn_{100-x}Pt_x$ (30 nm)/Pt(30 nm)/Cr (10 nm)/MgO(001) films, where $x=11$, 14, and 20, were prepared by the molecular beam epitaxy (MBE) method at room temperature. The $Mn_{100-x}Pt_x$ layer was deposited prior to the NiFe or CoFe layer in order to measure the XMCD signal of the AF layer by using a surface-sensitive TEY method. The $Mn_{100-x}Pt_x$ layer was deposited by coevaporation from independently controlled electron beam heated Mn and Pt sources, and the $Ni_{80}Fe_{20}$ or $Co_{90}Fe_{10}$ layer was deposited from an alloy source. The NiFe or CoFe and MnPt layers were grown applying a magnetic field of 100 Oe parallel to the [100] direction. After the growth, the bilayers were annealed at 200 °C in a vacuum below 2×10^{-5} Pa under a magnetic field of 850 Oe parallel to the [100] direction. The structure was characterized by *in situ* reflection high energy electron diffraction (RHEED) and *ex situ* x-ray diffraction (XRD) (Cu $K\alpha$). Magnetic properties were measured using an alternating gradient magnetometer (AGM) and a torque magnetometer at room temperature. The torque curves were measured applying a magnetic field of 15 kOe which is a field large enough to saturate the NiFe or CoFe. The XMCD were taken at the beam line BL25SU (Ref. 18) of the SPring-8 in Hyogo, Japan. The degree of circular polarization of the incident x ray is $P_c=0.998$. The helicity of the circular polarized x ray was switched at 1 Hz by twin helical undulators.[19] The element-specific hysteresis loops were measured by taking the XMCD signal at Mn and Fe or Co L_3 edges, sweeping an external field in the range of ±1.9 T.[20] The angle of the incident x ray was at 25° in relation to the sample surface, and its projection onto the surface was parallel to the easy direction of the unidirectional anisotropy. The external field was applied at 15° to the sample surface and its projection was parallel to the easy direction of the unidirectional anisotropy. If the samples are fully saturated by a sufficiently large external field, sample magnetization is oriented along 10° from the incident x rays.

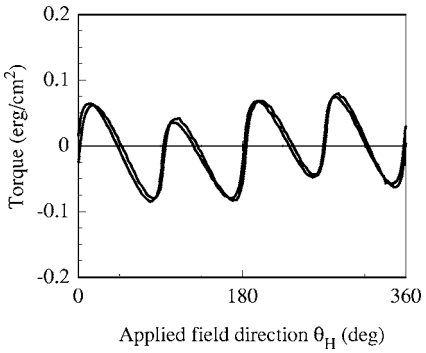

FIG. 1. In-plane torque curve of bottom-type NiFe/$Mn_{80}Pt_{20}$ bilayer with (001) orientation. θ_H is the angle between direction of the applied field and the [100] direction of the MnPt.

III. RESULTS AND DISCUSSIONS

As revealed by RHEED patterns, it was confirmed that the $Mn_{100-x}Pt_x$ and NiFe (CoFe) were epitaxially grown on the Pt/Cr/MgO(001) substrate. XRD profiles showed the diffraction peaks from the fundamental fcc of MnPt and NiFe (CoFe), and no superlattice peaks were evident. These results are almost the same as those previously reported,[16] and suggest that the MnPt, NiFe, and CoFe layers have a (001)-oriented disordered fcc structure. The difference in structure between the present bottom-type and the previous top-type bilayers was the grain size of $Mn_{100-x}Pt_x$. The bottom-type $Mn_{100-x}Pt_x$ exhibited a larger grain size of typically ~15 nm than the top type of ~10 nm. This may be due to the lattice mismatch of the $Mn_{100-x}Pt_x$ and its underlayers, which is estimated to be 3% for the bottom type while 7% for the top type.

As a typical in-plane torque curve for the bottom-type NiFe/Mn–Pt, the data for the NiFe/$Mn_{86}Pt_{14}$ bilayer annealed at 200 °C are shown in Fig. 1. Previously reported top-type Mn–Pt/NiFe bilayers[17] exhibited a large fourfold component of 0.05 erg/cm^2, which was comparable to the onefold component of 0.06 erg/cm^2, which corresponds to the unidirectional anisotropy. The bottom-type sample has almost the same fourfold anisotropy, while the small onefold component compared to the top-type sample, as seen in Fig. 1. For bottom-type bilayers, heat treatment is necessary to induce exchange biasing. The present small exchange bias field is probably due to the low annealing temperature of 200 °C, but a further increase of annealing temperature will lead to a decrease of exchange coupling, which was already observed in the preliminary experiment for top-type $Mn_{100-x}Pt_x$/NiFe epitaxial bilayers.

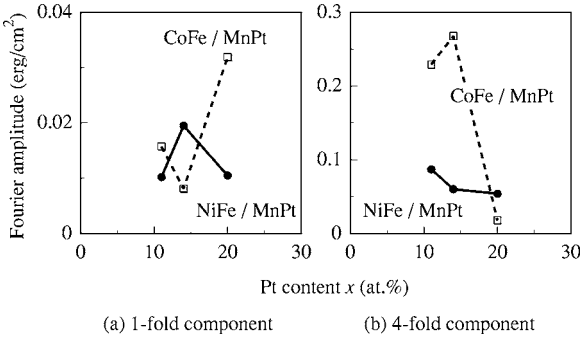

FIG. 2. One- and fourfold components estimated from the torque curves as a function of Pt content x in the $Mn_{100-x}Pt_x$ layer. The closed circles and open squares represent the data for NiFe/MnPt and CoFe/MnPt, respectively.

Figure 2 shows the one- and fourfold components estimated from the in-plane torque curves (for unit area of bilayers) as a function of Pt content x for the annealed $NiFe/Mn_{100-x}Pt_x$ and $CoFe/Mn_{100-x}Pt_x$ bilayers. Both $NiFe/Mn_{100-x}Pt_x$ and $CoFe/Mn_{100-x}Pt_x$ have large fourfold and small onefold components. These large fourfold components originate from the cubic anisotropy of the $Mn_{100-x}Pt_x$ because these values are much larger than those estimated for 3 nm NiFe and CoFe single layers of 1.6×10^{-3} and 1.1×10^{-2} erg/cm^2, respectively. On the other hand, the onefold component was small compared to the fourfold component and showed different Pt content dependence from that of the fourfold component. The small onefold component, i.e., unidirectional anisotropy, may be due to the low annealing temperature of 200 °C, as previously mentioned.

Figure 3 shows (a) x-ray absorption spectra (XAS) and (b) XMCD spectra for annealed $CoFe/Mn_{89}Pt_{11}$ taken at the Co and Mn $2p$-$3d$ excitation regions. The absorption spectra were obtained by averaging the absorption spectra measured for right and left circular polarized x rays. The absorption spectra are normalized so that the L_3 edge jump is equal to unity, as shown in Fig. 3(a). An XMCD spectrum is determined by the difference of the normalized absorption spectra between right and left polarized x rays. Even though no protective layer is deposited on the bilayer to obtain an XMCD signal from Mn–Pt layer with a high signal/noise (S/N) ratio,

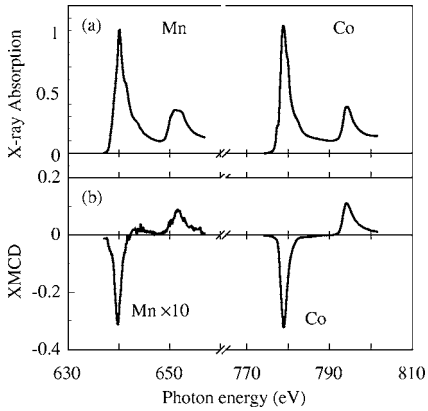

FIG. 3. (a) X-ray absorption and (b) XMCD spectra measured for $CoFe/Mn_{89}Pt_{11}$ taken at the Co and Mn $2p$-$3d$ excitation regions. The absorption spectra are normalized so that the L_3 edge jump is equal to unity.

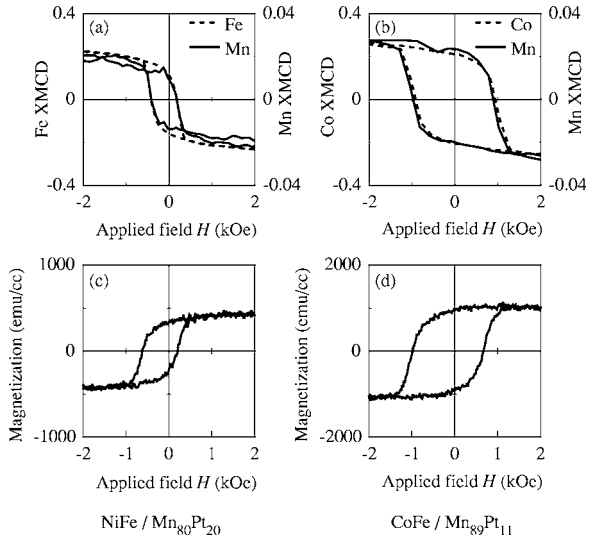

FIG. 4. Element-specific hysteresis loops for bottom-type (a) $NiFe/Mn_{86}Pt_{14}$ and (b) $CoFe/Mn_{89}Pt_{11}$. The solid and the dashed lines represent the hysteresis loops taken at the Mn and Fe (Co) L_3 edges, respectively. Hysteresis loops for bottom-type (c) $NiFe/Mn_{89}Pt_{11}$ and (d) $CoFe/Mn_{89}Pt_{11}$ measured by AGM are also shown for comparison.

Co XAS does not show significant multiplet structures, which is observed in CoO,[21] and Mn XAS exhibits almost the same spectral shape as does metallic Mn XAS.[22] This means that the oxidization of the bilayer surface is not significant, and the Mn–Pt layer is completely protected from oxidization. As seen in Fig. 3(b), XMCD was observed not only for the Co edge but also for the Mn edge. Based on the sign of XMCD signal for Mn and Co edges, the uncompensated Mn moment was found to couple ferromagnetically with the Co moment in the same manner as Co/MnIr reported by Ohldag *et al.*[13] The XMCD signal at the Mn edge suggests the existence of the uncompensated Mn moment at the interface between the CoFe and MnPt layers. Mitsumata *et al.* calculated the spin configurations of the F/AF bilayers for AF layer with disordered fcc structure and reported that an uncompensated moment of AF will appear near the F/AF interface[9] as a result of the rotation of AF spins from their original directions, i.e., the formation of the domain wall in AF.

Figure 4 shows the element-specific hysteresis loops for (a) the $NiFe/Mn_{80}Pt_{20}$ and (b) the $CoFe/Mn_{89}Pt_{11}$ bilayers after annealing. The solid and dashed lines represent the hysteresis loops taken at the Mn and Fe (or Co) L_3 edges, respectively. As a comparison, the hysteresis loops for the annealed $NiFe/Mn_{80}Pt_{20}$ and $CoFe/Mn_{89}Pt_{11}$ bilayers measured by AGM are shown in Figs. 4(c) and 4(d), respectively. The present bottom-type NiFe/MnPt has large coercivity (H_c) and a small exchange bias field (H_{ex}) compared to the previous top-type MnPt/NiFe bilayers.[16,17] The exchange biasing was along the [100] direction which is parallel to the applied field during the deposition and annealing. The saturation magnetizations of NiFe/MnPt and CoFe/MnPt were 480 and 1050 emu/cc, respectively, which are about 70% of those of bulk NiFe and CoFe. This is due to the surface oxidization of the ferromagnetic layer; however, the interface is completely protected from oxidization, as discussed above.

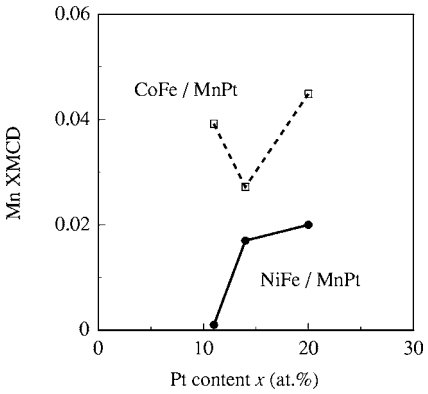

FIG. 5. Mn XMCD intensities estimated from element-specific hysteresis loops. The closed circles and open squares represent the data for NiFe/MnPt and CoFe/MnPt, respectively.

The element-specific hysteresis loops have almost the same H_c and H_{ex} as do the corresponding hysteresis loops taken by AGM. This means that the uncompensated Mn moment is strongly coupled with the adjacent ferromagnetic Co moment and rotates directionally with the Fe (or Co) moment. The gradual increase of the Fe (or Co) and Mn XMCD signals at the high field can be attributed to the field's application of 15° from the film's surface. The saturation value of the Mn XMCD contrast of ~0.03 at the L_3 edge is much smaller than that of Co (0.4), as shown in Fig. 4. If fully polarized Mn XMCD is assumed to be 0.55, as observed in Mn for ferromagnetic $MnPt_3$,[23] which were data obtained at the same facility as that of the present experiments, the present uncompensated Mn moment is estimated to be around 5% of the Mn moment. With regard to a vertical shift of the XMCD loop for Mn as pointed out by Ohldag *et al.*,[13] we did not observe obvious shifts of the loops for our bilayers, as shown in Figs. 4(a) and 4(b). Thus, we focus our interest in more detail on the amplitude of Mn XMCD loops for the $NiFe/Mn_{100-x}Pt_x$ and $CoFe/Mn_{100-x}Pt_x$ bilayers. The variation of Mn XMCD intensities with Pt content x is shown in Fig. 5. The variations of the Mn XMCD signal for both $NiFe/Mn_{100-x}Pt_x$ and $CoFe/Mn_{100-x}Pt_x$ are similar to the corresponding onefold components of the torque curves shown in Fig. 2(a), and if we focus on each system ($NiFe/Mn_{100-x}Pt_x$ or $CoFe/Mn_{100-x}Pt_x$), a larger XMCD was obtained for samples exhibiting a smaller fourfold anisotropy. Furthermore, the Mn XMCD intensities of $CoFe/Mn_{100-x}Pt_x$ are larger than those of $NiFe/Mn_{100-x}Pt_x$. We consider that the uncompensated moment of Mn is due to a domain wall formed in the AF layers as calculated in a disordered AF/F system,[9] and if so, the Mn moment is thought to be affected both by the exchange coupling at the F/AF interface and the cubic anisotropy of AF because the domain wall results from the balance of the exchange coupling and the domain wall energy of AF. In our system, the fourfold anisotropy originates from the F layer exchange coupled with $Mn_{100-x}Pt_x$ and is considered to reflect the cubic anisotropy of $Mn_{100-x}Pt_x$. In this framework, the increase of the XMCD intensity may be understood as the increase of the wall width in AF resulting from the increase of exchange coupling at F/AF or the decrease of fourfold anisotropy in $Mn_{100-x}Pt_x$.

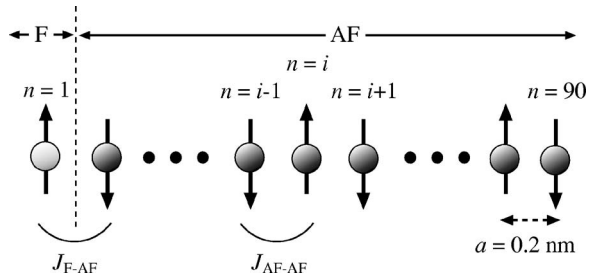

FIG. 6. Schematic of the assumed laminated spin structure. The circles of $n=1$ and $2 \leqslant n \leqslant 90$ represent F and AF spins, respectively. Positive $J_{F\text{-}AF}$, negative $J_{AF\text{-}AF}$, and cubic anisotropy of K_{AF} were assumed. The calculation step was set to $a=0.2$ nm.

In order to discuss the correlation between the Mn XMCD intensities and the AF wall width at the interface, we performed a simulation assuming a laminated AF spin structure, as illustrated in Fig. 6. The spins were assumed to be restricted in the film plane and the easy directions of AF spins were set as 0°, 90°, −90°, and 180° from the MnPt[100] direction. The spin of layer number $n=1$ represents the direction of F spin and was assumed to be parallel to the external field. The spins of $2 \leqslant n \leqslant 90$ represent AF spins, and in the calculation the spacing of the layers was set to be $a=0.2$ nm. The intermixing at the interface was not taken into account. The energy stored in AF spins is given by the sum of the exchange coupling with adjacent spins and the cubic anisotropy of AF as follows:

$$E = \sum_{n=2}^{90} [-J_{n,n-1} \cos(\theta_n - \theta_{n-1}) + K_{AF} a \cos 4\theta_n], \qquad (1)$$

where K_{AF} is the anisotropy constant of AF and $J_{n,n-1}$ is the exchange constant to the adjacent spin. We simply assumed a negative exchange coupling between AF spins, $J_{AF\text{-}AF}$, and the positive coupling of F and AF, $J_{AF\text{-}F}$. Typically we set $J_{AF\text{-}AF}$ to -50 erg/cm^2, which corresponds to the exchange stiffness of $aJ_{AF\text{-}AF}=10^{-6}$ erg/cm. The spin configuration was calculated by finding θ_n $(2 \leqslant n \leqslant 89)$ numerically as to minimize the energy E. The spin direction of $n=90$, θ_{90}, was fixed in the calculation.

Figure 7 shows the wall structure in the AF layer calculated for (a) $2\sqrt{aJ_{AF\text{-}AF}K_{AF}}=2$ ergs/cm^2, $J_{F\text{-}AF}=4$ ergs/cm^2 and (b) $2\sqrt{aJ_{AF\text{-}AF}K_{AF}}=2$ ergs/cm^2, $J_{F\text{-}AF}=2$ ergs/cm^2. The applied field direction, i.e., θ_1, was set to 0° parallel to MnPt-100] and 180° for the upper and lower figures, respectively. The figures are the results for the case of the initial value of $\theta_2=90°$. When the θ_1 is set to 0° shown in the upper of Fig. 7(a), the AF spins for $2 \leqslant n < 30$ rotate from their original directions of 90° or −90° due to the exchange coupling at the F/AF interface and form a domain wall. The AF spins for $n > 30$ are simulated to point 90° or −90° and the neighboring spins align antiferromagnetically. When the θ_1 is switched, the AF spins for $2 \leqslant n < 30$ rotate with θ_1, as shown in the lower half of Fig. 7(a). The wall becomes relatively obscure in AF when the $J_{F\text{-}AF}$ is reduced, keeping the domain wall energy $2\sqrt{aJ_{AF\text{-}AF}K_{AF}}$ constant of 2 ergs/cm^2, as shown in Fig. 7(b). The penetration of the wall is dependent mainly on the ratio of $J_{F\text{-}AF}$ and $2\sqrt{aJ_{AF\text{-}AF}K_{AF}}$. The

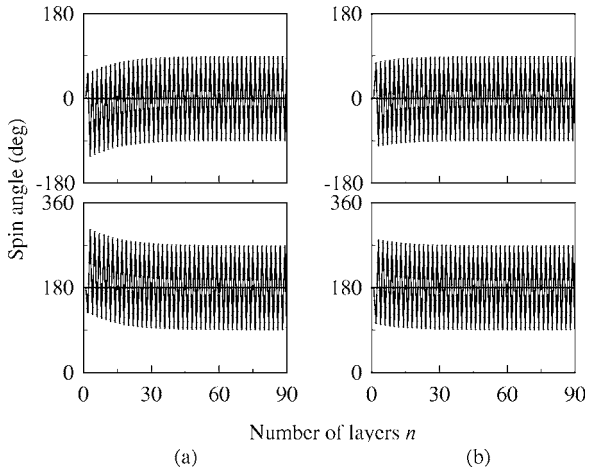

FIG. 7. Spin alignment calculated by minimizing the AF total energy of E for (a) $J_{\text{F-AF}}=4$ ergs/cm^2, $2\sqrt{aJ_{\text{AF-AF}}K_{\text{AF}}}=2$ ergs/cm^2 and (b) $J_{\text{F-AF}}=2$ ergs/cm^2, $2\sqrt{aJ_{\text{AF-AF}}K_{\text{AF}}}=2$ ergs/cm^2. Upper and lower figures are the results for the applied field direction, i.e., θ_1 of 0° (parallel to MnPt[100]) and 180°, respectively.

larger $J_{\text{F-AF}}/2\sqrt{aJ_{\text{AF-AF}}K_{\text{AF}}}$, in other words AF materials having a higher Néel temperature and/or larger crystalline anisotropy, results in the less penetration of the wall, as shown in Fig. 7.

The uncompensated moment at F/AF interface, which is proportional to XMCD signal, is calculated by taking into account the contribution of AF spins to the XMCD signal with exponential decay as follows:

$$\sum_{i=1}^{44}(\cos\theta_{2i}+\cos\theta_{2i+1}) \times\exp[-(2ia+t_{\text{F}})/d_p]/\sum_{i=1}^{44}2\exp[-(2ia+t_{\text{F}})/d_p], \qquad (2)$$

where the F layer thickness is $t_{\text{F}}=3$ nm and the XMCD probing depth is simply assumed to be $d_p=3$ nm.[24] We averaged the uncompensated moments calculated for $\theta_{90}=0°$, 90°, −90°, and 180°. Figure 8 shows the calculated uncompensated moment (normalized value) at the F/AF as a function of $J_{\text{F-AF}}/2\sqrt{aJ_{\text{AF-AF}}K_{\text{AF}}}$. The figure was obtained by varying $J_{\text{F-AF}}$ from 1 to 4 erg/cm^2 while fixing $J_{\text{AF-AF}}=$

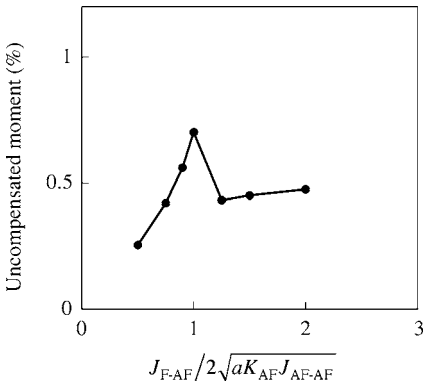

FIG. 8. Normalized uncompensated moments at the F/AF interface calculated by using Eq. (2) as a function of $J_{\text{F-AF}}/2\sqrt{aJ_{\text{AF-AF}}K_{\text{AF}}}$. The figure is the calculated result for $J_{\text{AF-AF}}=-50$ ergs/cm^2 and $aK_{\text{AF}}=0.02$ ergs/cm^2.

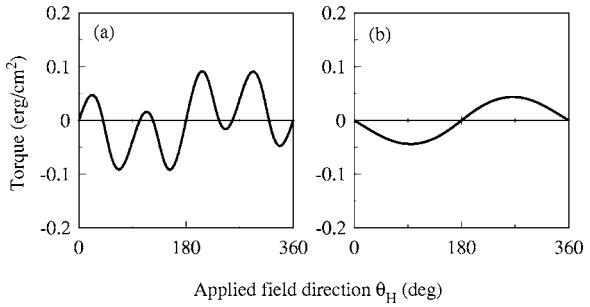

FIG. 9. Calculated in-plane torque curves for (a) $J_{\text{F-AF}}=1.8$ ergs/cm^2, $2\sqrt{aJ_{\text{AF-AF}}K_{\text{AF}}}=1.9$ ergs/cm^2 and (b) $J_{\text{F-AF}}=1.8$ ergs/cm^2, $2\sqrt{aJ_{\text{AF-AF}}K_{\text{AF}}}=3.2$ ergs/cm^2.

-50 ergs/cm^2 and $aK_{\text{AF}}=0.02$ ergs/cm^2. In the figure, the uncompensated moments were found to increase with increasing $J_{\text{F-AF}}/2\sqrt{aJ_{\text{AF-AF}}K_{\text{AF}}}$ up to $J_{\text{F-AF}}/2\sqrt{aJ_{\text{AF-AF}}K_{\text{AF}}}=1$, which results from the penetration of the wall in the AF. The drop of the uncompensated moment for $J_{\text{F-AF}}/2\sqrt{aJ_{\text{AF-AF}}K_{\text{AF}}}>1$ is due to the limited probing depth. For $J_{\text{F-AF}}>2\sqrt{aJ_{\text{AF-AF}}K_{\text{AF}}}$, the AF domain wall deeply penetrates into the AF and the wall thickness becomes larger than the probing depth, which results in the decrease of the uncompensated moment within the probing depth. The calculated uncompensated moment is around 0.5%, which is smaller than the experimental moments around 5% estimated by assuming that fully polarized Mn has an XMCD contrast of 0.55.[23] This deviation may be due to the assumed spin structure in the AF layer. We assumed here that the AF layer has a collinear spin structure; however, a more precise spin structure, such as a triangle configuration as calculated by Mitsumata *et al.*,[9] will be necessary for a quantitative discussion.

The in-plane torque curve can be calculated by differentiating the total energy, i.e., the sum of E_n in Eq. (1), with respect to the direction of the external field θ_1. In order to fit the calculated result to the experimental curve, four AF crystal domains whose easy directions are along 0°, 90°, −90°, and 180° are assumed and the AF domains having 0° easy direction is assumed to have a 10% larger area than do the other three domains. The applied field during the growth and/or the annealing may induce such an unbalance of the area in the F/AF bilayer.

Figure 9(a) shows the torque curve calculated for $2\sqrt{aJ_{\text{AF-AF}}K_{\text{AF}}}=1.9$ ergs/cm^2 and $J_{\text{F-AF}}=1.8$ ergs/cm^2, and it was found that the calculated curve reproduces the coexistence of the one- and the fourfold components and agrees well with the experimental curve shown in Fig. 1. The calculated torque curve suggests that the coexistence of the one- and the fourfold components, observed experimentally in our (001)-oriented bilayers, may originate from the domain wall formed in the MnPt antiferromagnetic layer. With increasing $2\sqrt{aJ_{\text{AF-AF}}K_{\text{AF}}}$, the fourfold component in the torque curve was significantly reduced, as seen in Fig. 9(b) ($2\sqrt{aJ_{\text{AF-AF}}K_{\text{AF}}}=3.2$ ergs/cm^2, $J_{\text{F-AF}}=1.8$ ergs/cm^2), since the formation of the wall was prohibited by the large wall energy of the AF, and the torque curve exhibited a behavior similar to that expected under the coherent rotation model.[3] If we assume a large wall energy of $Mn_{80}Ir_{20}$ compared to the present $Mn_{100-x}Pt_x$, since the $Mn_{80}Ir_{20}$ exhibits higher T_N

than does the $Mn_{80}Pt_{20}$,[25,26] the torque curve observed for the $Mn_{80}Ir_{20}$/NiFe bilayers,[10,27] which is explained by the coherent rotation model, may also be explained by the model presented here.

IV. CONCLUSION

(001)-oriented bottom-type NiFe/$Mn_{100-x}Pt_x$ and CoFe/$Mn_{100-x}Pt_x$ epitaxial bilayers were grown using MBE method. The bilayers with a Pt content x of around 10 at. % exhibited both one- and fourfold anisotropies and the fourfold component in the torque curve for the CoFe/MnPt was larger than that of the NiFe/MnPt. The uncompensated Mn moment at the NiFe/MnPt and CoFe/MnPt interfaces was confirmed by XMCD measurements. A larger Mn XMCD was observed for CoFe/MnPt than for NiFe/MnPt. Calculation assuming a laminated AF spin structure suggests that the uncompensated Mn moment results from a domain wall formed in the MnPt layer exchange coupled with the adjacent F layer and the uncompensated moment increases with the increasing strength of the exchange coupling at the F/AF interface. Furthermore, this model was found to explain the coexistence of the one- and the fourfold components in the in-plane torque curve, and it was suggested that the exchange anisotropy of our CoFe/MnPt and NiFe/MnPt originates from the domain wall near the F/AF interface.

ACKNOWLEDGMENTS

The authors would like to thank M. Kumazawa of Nagoya University for his experimental assistance and Dr. T. Muro of JASRI/SPring-8 for his technical support during the XMCD measurement. This experiment was carried out with the approval of the SPring-8 Program Advisory Committee (Proposal No. 2003B0540-NSc-np-Na, 2005A0290-NSc-np).

[1]R. F. C. Farrow, R. F. Marks, S. Gider, A. C. Marley, S. S. P. Parkin, and D. Mauri, J. Appl. Phys. **81**, 4986 (1997).
[2]H. Kishi, Y. Kitade, Y. Miyake, A. Tanaka, and K. Kobayashi, IEEE Trans. Magn. **32**, 3380 (1996).
[3]W. H. Meiklejohn and C. P. Bean, Phys. Rev. **105**, 904 (1957).
[4]D. Mauri, H. C. Siemann, P. S. Bagus, and E. Kay, J. Appl. Phys. **62**, 3047 (1987).
[5]A. P. Malozemoff, Phys. Rev. B **35**, 3679 (1987).
[6]N. C. Koon, Phys. Rev. Lett. **78**, 4865 (1997).
[7]T. C. Shulthes and W. H. Butler, Phys. Rev. Lett. **81**, 4516 (1998).
[8]J. Nogués and I. K. Schuller, J. Magn. Magn. Mater. **192**, 203 (1999).
[9]C. Mitsumata, A. Sakuma, and K. Fukamichi, Phys. Rev. B **68**, 014437 (2003).
[10]M. Tsunoda, Y. Tsuchiya, T. Hashimoto, and M. Takahashi, J. Appl. Phys. **87**, 4375 (2000).
[11]K. Nishioka, C. Hou, H. Fujiwara, and R. D. Metzger, J. Appl. Phys. **80**, 4528 (1996).
[12]Y. J. Tang *et al.*, Phys. Rev. B **62**, 8654 (2000).
[13]H. Ohldag, A. Scholl, F. Nolting, E. Arenholz, S. Maat, A. T. Young, M. Carey, and J. Stöhr, Phys. Rev. Lett. **91**, 017203 (2003).
[14]T. Eimüller, T. Kato, T. Mizuno, S. Tsunashima, C. Quitmann, T. Ramsvik, S. Iwata, and G. Schütz, Appl. Phys. Lett. **85**, 2310 (2004).
[15]K. Takano, R. H. Kodama, A. E. Berkowitz, W. Cao, and G. Thomas, Phys. Rev. Lett. **79**, 1130 (1997).
[16]T. Kume, Y. Sugiyama, T. Kato, S. Iwata, and S. Tsunashima, J. Appl. Phys. **93**, 6599 (2003).
[17]T. Kume, T. Kato, S. Iwata, and S. Tsunashima, J. Magn. Magn. Mater. **272–276**, E827 (2004).
[18]Y. Saitoh *et al.*, J. Synchrotron Radiat. **5**, 542 (1998).
[19]T. Hara, K. Shirasawa, M. Takeuchi, A. Hiraya, and H. Kitamura, Nucl. Instrum. Methods Phys. Res. A **498**, 496 (2003).
[20]T. Nakamura, T. Muro, F. Z. Guo, T. Matsushita, T. Wakita, T. Hirono, Y. Takeuchi, and K. Kobayashi, J. Electron Spectrosc. Relat. Phenom. **144–147**, 1035 (2005).
[21]F. M. F. de Groot, M. Aggate, J. van Elp, G. A. Sawatzky, Y. J. Ma, C. T. Chen, and F. Sette, J. Phys.: Condens. Matter **5**, 2277 (1993).
[22]S. Imada, T. Muro, T. Shishidou, S. Suga, H. Maruyama, K. Kobayashi, H. Yamazaki, and T. Kanomata, Phys. Rev. B **59**, 8752 (1999).
[23]T. Kato, Y. Fujiwara, S. Iwata, and S. Tsunashima, J. Magn. Magn. Mater. **240**, 517 (2002).
[24]T. J. Regan, H. Ohldag, C. Stamm, F. Nolting, J. Lüning, J. Stöhr, and R. L. White, Phys. Rev. B **64**, 214422 (2001).
[25]T. Yamaoka, M. Mekata, and H. Takaki, J. Phys. Soc. Jpn. **36**, 438 (1974).
[26]E. Krén, Phys. Lett. **21**, 383 (1966).
[27]T. Kume, T. Kato, S. Iwata, and S. Tsunashima, J. Magn. Magn. Mater. **286**, 243 (2005).